

---

---

# Semiautomatic Region-of-Interest Validation at the Femur in $^{18}\text{F}$ -Fluoride PET/CT

Tanuj Puri<sup>1,2</sup>, Glen M. Blake<sup>3</sup>, Kathleen M. Curran<sup>2</sup>, Hamish Carr<sup>4</sup>, Amelia E.B. Moore<sup>3</sup>, Niall Colgan<sup>2,5</sup>, Martin J. O'Connell<sup>6</sup>, Paul K. Marsden<sup>1</sup>, Ignac Fogelman<sup>3</sup>, and Michelle L. Frost<sup>3</sup>

<sup>1</sup>PET Imaging Centre, Imaging Sciences and Biomedical Engineering, St. Thomas' Hospital, King's College London, London, United Kingdom; <sup>2</sup>School of Medicine and Medical Sciences, University College Dublin, Dublin, Ireland; <sup>3</sup>Osteoporosis Screening and Research Unit, Imaging Sciences and Biomedical Engineering, Guy's Hospital, King's College London, London, United Kingdom; <sup>4</sup>University of Leeds, Leeds, United Kingdom; <sup>5</sup>College of Medicine, Swansea University, Wales, United Kingdom; and <sup>6</sup>Mater Misericordiae University Hospital, Dublin, Ireland

The assessment of regional skeletal metabolism using  $^{18}\text{F}$ -fluoride PET ( $^{18}\text{F}$ -PET) requires segmentation of the tissue region of interest (ROI). The aim of this study was to validate a novel approach to define multiple ROIs at the proximal femur similar to those used in dual x-ray absorptiometry. Regions were first drawn on low-dose CT images acquired as a routine part of the PET/CT study and transferred to the  $^{18}\text{F}$ -PET images for the quantitative analysis of bone turnover. **Methods:** Four healthy postmenopausal women with a mean age of 65.1 y (range, 61.8–70.0 y), and with no history of metabolic bone disorder and not currently being administered treatment affecting skeletal metabolism, underwent dynamic  $^{18}\text{F}$ -PET/CT at the hip with an injected activity of 180 MBq. The ROIs at the proximal femur included femoral shaft, femoral neck, and total hip and were segmented using both a semiautomatic method and manually by 8 experts at manual ROI delineation. The mean of the 8 manually drawn ROIs was considered the gold standard against which the performances of the semiautomatic and manual methods were compared in terms of percentage overlap and percentage difference. The time to draw the ROIs was also compared. **Results:** The percentage overlaps between the gold standard and the semiautomatic ROIs for total hip, femoral neck, and femoral shaft were 86.1%, 37.8%, and 96.1%, respectively, and the percentage differences were 14.5%, 89.7%, and 4.7%, respectively. In the same order, the percentage overlap between the gold standard and the manual ROIs were 85.2%, 39.1%, and 95.2%, respectively, and the percentage differences were 19.9%, 91.6%, and 12.2%, respectively. The semiautomatic method was approximately 9.5, 2.5, and 67 times faster than the manual method for segmenting total-hip, femoral-neck, and femoral-shaft ROIs, respectively. **Conclusion:** We have developed and validated a semiautomatic procedure whereby ROIs at the hip are defined using the CT component of an  $^{18}\text{F}$ -PET/CT scan. The percentage overlap and percentage difference results between the semiautomatic method and the manual method for ROI delineation were similar. Two advantages of the semiautomatic method are that it is significantly quicker and eliminates some of the variability associated with operator or reader input. The tube current used for the CT scan

was associated with an effective dose 8 times lower than that associated with a typical diagnostic CT scan. These results suggest that it is possible to segment bone ROIs from low-dose CT for later transfer to PET in a single PET/CT procedure without the need for an additional high-resolution CT scan.

**Key Words:**  $^{18}\text{F}$ -PET/CT; femur; bone; region of interest; validation

**J Nucl Med Technol 2012; 40:168–174**

DOI: 10.2967/jnmt.111.100107

---

**T**he assessment of regional bone turnover is important in the understanding of the pathophysiology of metabolic bone diseases such as osteoporosis. Studies of the differential response between cortical and trabecular bone to aging, disease, and treatment may provide a better understanding of mechanisms of action of novel treatments currently being developed for osteoporosis (1,2) and allow insight into the role of regional bone turnover as a risk factor for fracture. The functional imaging technique of dynamic  $^{18}\text{F}$ -fluoride PET ( $^{18}\text{F}$ -PET) offers a noninvasive method for quantifying bone turnover at specific sites in the skeleton, such as the spine and hip. The use of this technique has been validated by comparison with the gold standard of bone biopsy (3,4).

To quantify bone turnover at the femur, dynamic  $^{18}\text{F}$ -PET analysis involves parameter estimation from mathematic modeling of the  $^{18}\text{F}$ -fluoride kinetics using an input function (i.e., tracer concentration in arterial plasma) from the femoral artery and time–activity curves (i.e., tracer concentration over time) from appropriately defined regions of interest (ROI) in the skeleton (5,6). The definition of ROIs on the PET images themselves is difficult because of low spatial resolution, high noise, low tracer uptake, and anatomic landmarks or boundaries that are difficult to visualize. Moreover, the manual ROI definition by experts is a time-consuming process and is susceptible to high variability.

The introduction of PET/CT systems gives the option of automatically segmenting bone ROIs from the CT images. Segmentation of bone from CT images is traditionally performed using thresholding based on Hounsfield units followed

---

Received Oct. 31, 2011; revision accepted Mar. 5, 2012.

For correspondence or reprints contact: Tanuj Puri, PET Imaging Centre, Imaging Sciences and Biomedical Engineering, St. Thomas' Hospital, King's College London, London, U.K.

E-mail: tanujpuri82@gmail.com

Published online Aug. 14, 2012.

COPYRIGHT © 2012 by the Society of Nuclear Medicine and Molecular Imaging, Inc.

by techniques such as connectivity or seeded region growing. In general, this approach is reasonably successful because the CT values of bone are greater than those of the surrounding tissues. However, automatic bone segmentation by a global thresholding technique is difficult in some regions such as the hip joint, in which individual bone structures such as the femoral neck and trochanter are physically contiguous. The problem becomes more challenging when one is relying on the low-dose CT scans acquired for a PET/CT study, because these provide lower-resolution images than those acquired using standard CT.

Several techniques have been proposed in the literature to automatically segment femur from pelvis, femoral head, or acetabulum on CT images (7–9). However, no studies have been performed to validate techniques to define ROIs at multiple sites within the femur, similar to those used in dual x-ray absorptiometry (DXA) (10). In addition, previous studies did not use these ROIs to generate time–activity curves from PET data at the femur for the quantitative analysis of bone turnover and did not allow for the separate segmentation of cortical and trabecular bone. And finally, previous CT images were acquired using a 10–15 times higher tube current to obtain a higher signal-to-noise ratio, thus exposing the patients to a high level of radiation (7,11–13).

The main aim of this study was to validate a novel semi-automatic and time-efficient approach to define the ROIs at multiple sites within the proximal femur on the CT dataset, similar to the ROIs used in DXA but extended to 3-dimensional space. We also investigated whether ROIs could be defined semiautomatically on the CT component of the PET/CT images for later transfer to the PET images to generate tissue time–activity curves for the dynamic quantification of bone turnover. The ROI segmentation from the semiautomatic method was validated against a gold standard generated from manual analysis by a group of experts (14,15) using percentage overlap and percentage volume difference.

## MATERIALS AND METHODS

### Subjects

A total of 4 postmenopausal women with a mean age of 65.1 y (range, 61.8–70.0 y) who had volunteered to participate in an osteoporosis research study were recruited. All subjects had to be older than 50 y and at least 5 y past menopause. A medical history was taken for all subjects, including recent and current medication use. Subjects were excluded at screening if they had any diseases or were undergoing any treatments known to affect bone metabolism. Standard laboratory tests of serum calcium; albumin-corrected calcium; alkaline phosphatase; phosphate; liver, renal, and thyroid profiles; erythrocyte sedimentation rate; full blood count; and parathyroid hormone were assessed at screening and were found to be within normal limits for all subjects. DXA bone mineral density measurements at the lumbar spine (L1–L4), femoral neck, total hip, and whole body were performed using a Discovery device (Hologic Inc.). Women were not excluded if they were found to have low bone density (osteopenia) or osteoporosis using the criteria from the World Health Organization for diagnosing osteoporosis (16), but they could not commence any medication to reduce

fracture risk until all study visits had been completed. Of the 4 subjects, 2 were classified as nonosteoporotic and 2 were classified as osteoporotic on the basis of the lumbar spine and total-hip results. Informed written consent was obtained from each participant, and this project received ethical approvals from the University College Dublin Human Research Ethics Committee–Sciences (HREC-LS) Committee, St. Thomas Hospital Research Ethics Committee, and Administration of Radioactive Substances Advisory Committee.

### Image Acquisition and Reconstruction

Each subject underwent dynamic  $^{18}\text{F}$ -fluoride PET/CT at the hips performed on a Discovery ST scanner (GE Healthcare). Subjects were positioned to include the acetabulum to mid femur within the axial field of view of 15.4 cm. Subjects were injected with 180 MBq of  $^{18}\text{F}$ -fluoride. A large hook-and-loop strap was used to minimize patient movement during scan acquisition. The scanner start time was marked as the zero reference; the dose injection started at 10 s and was given over 10 s. A 10-mL saline flush was injected at 20 s and given over 10 s. Each 60-min dynamic scan resulted in  $24 \times 5$ ,  $4 \times 30$ , and  $14 \times 240$ -s time frames. The PET scans were reconstructed using filtered backprojection with a 6.3-mm Hanning filter. PET scans were attenuation-corrected using CT data. The attenuation-corrected PET images resulted in 47 slices in each frame (each slice,  $128 \times 128$  pixels), where each pixel measured  $2.734 \times 2.734 \times 3.27$  mm in the  $x$ ,  $y$ , and  $z$  directions, respectively. The CT dataset resulted in static scans of 47 slices (each slice,  $512 \times 512$  pixels), where each pixel measured  $0.977 \times 0.977 \times 3.27$  mm in the  $x$ ,  $y$ , and  $z$  directions, respectively. Other CT parameters included 4 detector slices; a pitch length of 1.5 mm, with a speed of 33 mm per rotation; a rotation time of 0.8 s; a tube current of 10-mA and 140-kV potential; a helical thickness of 5 mm; and a beam collimation of 20 mm.

### Semiautomatic ROI Definition Method

The study was performed using in-house software developed with MATLAB (The MathWorks). We started by noting that the proximal femur consists principally of 2 types of bone: a rigid outer shell formed of cortical bone and an internal honeycomb structure of trabecular bone. Where the cortical bone is thinnest, as, for example in the femoral neck, the risk of fracture is highest and is aggravated during the development of osteoporosis (17). We distinguished 3 ROIs in the proximal femur: the femoral shaft, femoral neck, and total hip. The ROIs were defined to be comparable with those used in DXA (Fig. 1) (10). Each of these regions poses different challenges; thus, we discuss each separately. The semiautomatic algorithm required 2 initial landmarks to be defined by the user (Fig. 1): the slice in which the greater trochanter meets the femoral neck, as represented by landmark 1 in Figure 1, and the slice in which the medial border of the lesser trochanter can be identified, as represented by landmark 2 in Figure 1.

After these 2 landmarks were manually defined, the semiautomatic algorithm was used to segment the 3 ROIs.

### Femoral-Shaft ROI

The region below the lesser trochanter is mainly cortical bone in the shape of a hollow cylinder. The annular ROI from this region ensures the inclusion of counts only from cortical bone. Moreover, the shaft is generally well aligned, vertically forming a hollow cylinder. The resulting cross-section of the cortical bone in the femoral shaft consists of an annulus, which was easily segmented with a threshold value of 50% of maximum intensity based on Hounsfield units. Slices 42–46 were used to segment the cortical

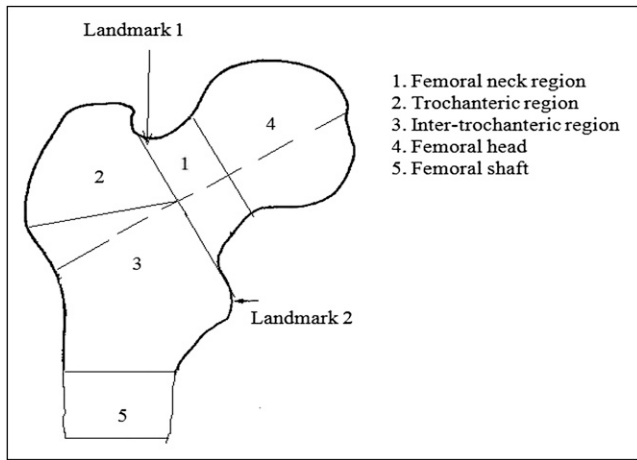


**FIGURE 1.** Two user-defined landmarks required for segmentation are shown by arrows. Different regions at femur are defined by numbers 1–5.

bone, excluding slice 47, in which the counts are reduced at the edge of the PET image. The segmented region is shown in Figure 2A.

### Femoral-Neck ROI

Unlike the femoral shaft, the femoral-neck axis is oblique to the axial, sagittal, and coronal slices. However, the distal border of the femoral neck is well defined by a line drawn between the 2 landmarks shown in Figure 1, and the proximal border is parallel with this line at a distance of 20 mm. Assuming that the femur has little or no rotation, we then extended these 2 parallel lines perpendicular to the coronal view to define 2 planes that separated the femoral neck from the intertrochanteric region and the femoral head, respectively. Within this region, the ratio of cortical to trabecular bone is generally insufficient to support threshold-based extraction, and we therefore used a region-growing method based on a user-specified seed point, which was placed inside an automatically marked region within the trabecular bone of the femoral neck. Because of the low resolution of the CT images, the femoral-neck ROI included a mixture of trabecular and cortical bone. The segmented region is shown in Figure 2B. Because the ROI is small and the cortical shell is thin, it was not possible to separate cortical and trabecular bone in this region.

### Total-Hip ROI

Once the proximal border of the femoral neck was defined, this border could also be used to define the total-hip ROI, which includes the femoral neck, the intertrochanteric region, the greater and lesser trochanters, and a portion of the femoral shaft distal to the femoral neck up to 1 cm below the lesser trochanter (Fig. 1). The segmentation of cortical bone involved a combination of iterative

thresholding and canny edge detection. The gaps in the boundary were joined using a dilation-and-erosion operation. The segmentation started from the slice in which the greater trochanter was first visible and ended 3 slices (1 cm) below the lesser trochanter (which is automatically calculated), ensuring the inclusion of most of the trabecular bone in the proximal femur as measured on a DXA scan. The segmented region is shown in Figure 2C.

### Manual Tracing

The manual ROIs were traced by 7 radiographers trained at ROI delineation and an expert medical physicist with mean imaging experience of 12.7 y (range, 3–24 y).

All the manual ROIs were also drawn using MATLAB with identical physical conditions. Each dataset was manually traced once by each expert. The average of all manual ROIs was considered the gold standard (14,15). Femoral-shaft ROIs were drawn on slices 42–46. The total-hip ROIs were drawn from the slice in which the uppermost tip of the greater trochanter was first visualized up to 3 slices (1 cm) below the lesser trochanter. The femoral-neck ROIs were drawn where the trabecular bone was best visualized in the femoral-neck region, approximately 20 mm deep inside the neck toward the femoral head.

The ROIs were drawn on the left and right femurs on all 4 datasets. The time required to draw the ROIs was also recorded. The software displayed the CT data in axial and coronal planes, with fixed window width and window center to present the data with consistent visual effects or perception. The images were initially presented at a fixed zoom; however, users were given full control to zoom, unzoom, and pan the images further. The manual traces were permitted only on axial slices using a point-based method. An additional functionality was provided that mapped the ROIs drawn on axial data onto coronal slices. The target ROIs were explained to all observers, who were also provided with a guidance sheet describing them.

### ROI Validation

The semiautomatic ROI method was validated by comparison with the gold standard ROIs obtained by averaging the manual regions drawn by experts. The gold standard in our case was the average of all ROIs drawn by the experts. The average region was calculated as shown in Figure 3 (18). In this figure, we show 2 different examples of the average boundary being calculated from 2 overlapping ROIs using our algorithm. For 2 overlapping ROIs, the centroid of the 2 regions is calculated, and then from this common centroid the mid boundary of the 2 regions is marked over the whole circular range such that the distance between the boundary of the first region to the averaged boundary is equal to the distance between the boundary of the second region and the averaged boundary when measured along the same direction.

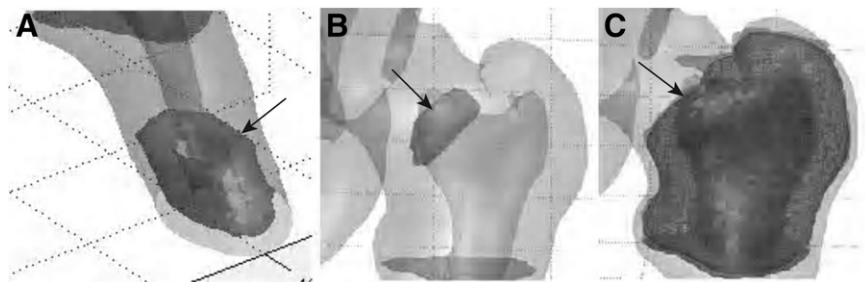


**FIGURE 2.** Segmented ROIs defined by semiautomatic technique. (A) Femoral-shaft ROI with cortical bone only forming hollow cylinder. (B) Femoral-neck ROI. (C) Total-hip ROI including trabecular and cortical bone of trochanter and femoral neck. ROIs are indicated by arrows. A color version of this figure is available as a supplemental file at <http://tech.snmjournals.org>.

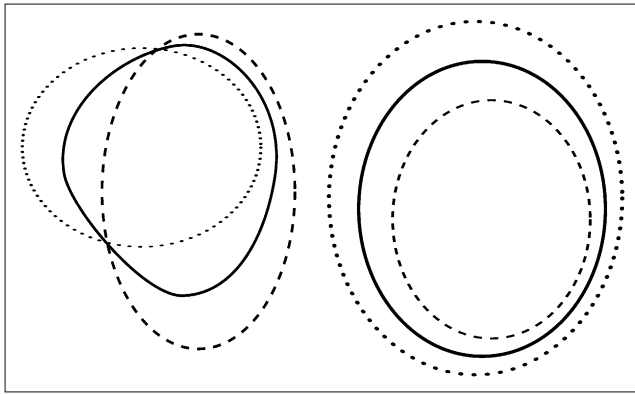


**FIGURE 3.** Two different examples of mean region (solid ovals) estimation using mean point-based distance between 2 regional boundaries (dashed ovals and dotted ovals). A color version of this figure is available as a supplemental file at <http://tech.snmjournals.org>.

### Statistical Analysis

We analyzed 3 different regional traces—namely, femoral shaft, femoral neck, and total hip—on the left and right hips for 4 subjects. Twenty-four volumes (3 ROIs × 8 datasets [including left and right sides]) were traced by each observer and our semiautomatic method. Therefore, a total of 216 volumes (24 × [8 observers + 1 semiautomatic]) were available for analysis. Percentage overlap, percentage difference, and time to draw the ROIs were used to examine the performance of the new method.

The dice similarity coefficient (DSC) (19) is an index for overlap-region analysis comparing the similarities between ROIs drawn by 2 different methods. For any 2 regions  $R_1$  and  $R_2$ , the DSC index can be defined as the ratio of overlap between the 2 regions and the mean of the 2 regions. The DSC ranges from zero, for complete disassociation, to unity, for perfect overlap between  $R_1$  and  $R_2$ .  $DSC \times 100$  gives the percentage overlap as in Equation 1.

$$\text{Percentage overlap } (R_1, R_2) = \frac{R_1 \cap R_2}{\left(\frac{R_1 + R_2}{2}\right)} \times 100. \quad \text{Eq. 1}$$

The values of DSC above 70% show clinically acceptable agreement between the 2 segmented regions (20–22). The DSC index is the most popular criterion used in the literature for ROI validation studies (23–25), as it is considered the special case of  $\kappa$ -statistics (21).

Interobserver variability was assessed using percentage volume difference, as described in Equation 2:

$$\text{Percentage difference } (R_1, R_2) = \frac{|R_1 - R_2|}{\left(\frac{R_1 + R_2}{2}\right)} \times 100, \quad \text{Eq. 2}$$

where percentage difference ranges from zero, for complete agreement, to 100%, for complete disagreement between  $R_1$  and

$R_2$  (14,25,26). The only disadvantage of using nonoverlapping-region analysis is that it is invariant to the spatial shift between the 2 regions; therefore, the difference is also reported in conjunction with DSC to calculate the interobserver variability.

We also measured the time required to draw the manual and semiautomatic ROIs generated by our algorithm to show the time saved over manual tracing of the regional boundaries.

### RESULTS

The mean and SD values of the percentage volume overlap and differences between the semiautomatically drawn ROIs and manual gold standards for total-hip, femoral-neck, and femoral-shaft regions are shown in Table 1. A higher value of percentage overlap and a lower value of percentage difference show stronger agreement and vice versa. Table 2 shows similar indices between the gold-standard ROI and each manually drawn ROI. The semiautomatic method showed better agreement with the gold standard than did the manual method in terms of percentage overlap for femoral-shaft and total-hip regions. The percentage differences between the gold standard and semiautomatic ROIs were less than the percentage differences between the gold standard and manual ROIs for all regions except the femoral neck. The time to draw the ROIs manually and semiautomatically is shown in Table 3. Our semiautomatic method was found to be approximately 67, 2.5, and 9.5 times faster, respectively, than the manual method for segmenting the femoral-shaft, femoral-neck, and total-hip ROIs.

Figure 4 shows the mean of time-activity curves generated from the femoral-shaft, femoral-neck, and total-hip regions after the ROIs were transferred to the dynamic PET/CT dataset.

### DISCUSSION

The technique of  $^{18}\text{F}$ -PET is a valuable research tool for the quantitative assessment of regional bone metabolism at clinically important sites such as the lumbar spine and hip. Studies using PET require ROIs to be drawn enclosing the boundary of the tissue that is to be quantified. The gold-standard method to define a region manually by an expert is time-consuming, susceptible to high variability, and not feasible in routine clinical practice. Therefore, semiautomatic or fully automatic methods are preferred. In this study, we defined multiple ROIs within the proximal femur semiautomatically and validated them against a gold standard defined by the average ROI drawn by 8 experts. We also compared the time to draw ROIs manually and semiautomatically by our new method.

**TABLE 1**  
Percentage Overlap and Differences Between Gold Standard and Semiautomatically Segmented ROIs

Gold standard vs. semiautomatic	Total hip		Femoral neck		Femoral shaft	
	Mean	SD	Mean	SD	Mean	SD
Percentage overlap	86.1	5.9	37.8	15.9	96.1	3.3
Percentage difference	14.5	12.5	89.7	44.2	4.7	6.0

**TABLE 2**  
Percentage Overlap and Differences Between Gold Standard (Mean of 8 Manually Drawn ROIs)  
and Manually Drawn ROIs (Each Separately Drawn Manual ROI)

Gold standard vs. manually drawn ROI	Total hip		Femoral neck		Femoral shaft	
	Mean	SD	Mean	SD	Mean	SD
Percentage overlap	85.2	42.9	39.1	24.3	95.2	47.8
Percentage difference	19.9	15	91.6	61.4	12.2	25.3

The manual ROI delineation on the PET scans is difficult because PET images have low spatial resolution, have low signal-to-noise ratio, show only metabolic activity on the scan, and do not give any structural information on the tissue or region. For these reasons, high-resolution CT images of the region under study might be required for the definition of ROIs and then for later transfer to PET data for quantification. However, we have shown that the use of PET/CT is simple, time-efficient, and cost-effective; limits patients to exposure to a relatively low radiation dose; and allows a single procedure without the need to obtain an additional CT scan for quantification of the PET data. The use of low-dose parameters for CT acquisitions with a tube current of 10 mA resulted in an effective dose to the subject of 0.8 mSv while providing enough contrast in the low-resolution CT scan for accurate segmentation of the bone tissue at the proximal femur. For diagnostic-quality CT scans of the pelvis with a tube current of 80 mA, the effective dose would have been 7 mSv, 8 times higher than the dose used in the present study.

The semiautomatically drawn ROIs were assessed by comparison with the gold standard in terms of the percentage overlap to show the strength of agreement. The semiautomatically segmented total-hip and femoral-shaft regions showed high overlap greater than the 70% figure for acceptable agreement, but the femoral neck had much poorer overlap (Table 1). The interoperator variability measured as percentage differences was higher for the manual method than the semiautomatic method for all 3 ROIs (Tables 1 and 2). The manual boundary definition might vary according to an individual's perception, giving a lower percentage overlap and larger percentage difference than boundaries drawn semiautomatically. The percentage overlap between the gold standard and each manual method was lower than that obtained between the gold standard and our method, showing the superiority of our semiautomatic algorithm over manual segmentation. The total-hip and femoral-shaft ROIs showed a small difference, but the results were much worse for the femoral neck.

The results expressed in Table 1 appear to show that the semiautomatic method failed to segment the femoral-neck ROI because the percentage overlap for this region did not reach the clinical acceptance level of 70% when assessed against the gold standard. However, this result was due to the high variability in drawing the manual femoral-neck boundaries on axial slices—as is clearly evident from Table 2 (percentage difference is 91.6)—making the average femoral-neck region obtained from manually drawn boundaries

unreliable. On visual inspection of the femoral-neck ROI drawn by each expert, we concluded that the semiautomatically defined ROIs were more reliable than those drawn manually (despite low percentage overlap and high percentage difference).

It is clear from Table 3 that ROIs within the femur are drawn more quickly using the semiautomatic method than the manual method. Measurement of standardized uptake values at these sites using the semiautomatic method could be useful in clinical routine, because previous studies have shown a good correlation between standardized uptake value and dynamic quantitative parameters obtained using non-linear regression at highly metabolically active skeletal sites (27–29).

Some studies have compared the volumes of automatically drawn ROIs and manually drawn ROIs in terms of Bland–Altman and correlation coefficients. We did not use this approach because 2 completely different ROI definitions can have exactly the same volume or perimeter, and comparing the volumes of different boundaries is not an adequate test, as was pointed out by Bourantas et al. (14).

Because the femoral-shaft ROI gives a measurement of pure cortical bone and the total-hip ROI gives a measurement of a mixture of trabecular and cortical bone—measurements that can help in understanding the metabolic differences in these 2 types of bones—these ROIs seem to be the best choice for measuring bone turnover for osteoporotic studies. Using these ROIs might also aid in measuring the differential response to certain drugs of both types of bones at the femur. The total-hip ROI is the largest region at the proximal femur that we measured, with the largest number of counts. Although it would be interesting to investigate the metabolic differences within the total-hip region by comparison with the metabolic responses of pure cortical and pure trabecular bone, because of the low resolution of the scanner it was not possible to segment the trabecular bone alone. The femoral-neck ROI is smaller and has fewer counts. This region also contains a mixture of 2 types of bone, but because most

**TABLE 3**  
Time to Draw ROIs Manually and Semiautomatically

Time (s)	Total hip		Femoral neck		Femoral shaft	
	Mean	SD	Mean	SD	Mean	SD
Semiautomatic	94.5	18.6	49.0	8.0	3.28	0.6
Manual	895.3	371.9	120.1	100.1	219.5	168.9

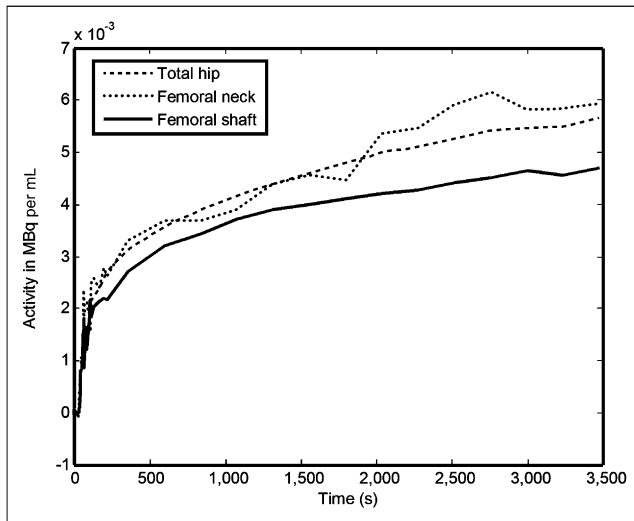


**FIGURE 4.** Mean time-activity curves generated from semiautomatically segmented ROIs. A color version of this figure is available as a supplemental file at <http://tech.snmjournals.org>.

fractures at the femur occur at the femoral neck, it might still be a useful region to study, even with the uncertainties associated with defining an ROI at this site.

Because ROIs on PET images are affected by partial-volume effects due to low resolution, it could be debated whether defining ROIs on CT images and then transferring them to PET images is suitable. In this regard, smaller regions (especially those that are < 2 times the spatial resolution of the PET scanner) would be affected by partial-volume effects the most. In this study, the size of total-hip and femoral-shaft ROIs was greater than twice the spatial resolution of the PET scanner. However, the method gave reasonable estimates of the bone time-activity curve (Fig. 4), and these estimates are expected to be better than those obtained through manual delineation on PET images, followed by thresholding (which would account only for regions with activity above a certain threshold).

The main limitation of this study was the small sample size, chosen because manual segmentation is time-consuming. Each expert took on average 45 min to draw all 3 ROIs (taking into account the time to handle the software, load the images, visualize the data, browse through the slices, map the ROIs drawn on axial slices to the sagittal plane, and save the ROI drawn) on 1 dataset, and therefore including more datasets in the study was not practical. To compensate for the small dataset, we increased the number of experts participating, thus giving a realistic evaluation of the interobserver variation and higher statistical significance for the derivation of the manual gold standard. The transfer of ROIs from CT to PET used mapping and alignment as a result of dual-modality PET/CT, and a previous study on the same scanner revealed a root-mean-square target-registration error of 6 mm for PET/CT alignment (30). Rigid-body PET/CT point-based registration performed better than did the PET/CT alignment and gave a root-mean-square target-registration error of 3 mm

(30). However, external markers were not used in the present study; therefore, PET/CT alignment was used for the transfer of segmented regions from CT to dynamic PET data.

## CONCLUSION

We have developed and validated a semiautomatic procedure whereby ROIs at the hip are defined using the CT component of an <sup>18</sup>F-PET/CT scan. The percentage overlap and percentage difference between the semiautomatic and the manual-definition methods for deriving ROIs were similar. Two advantages of the semiautomatic method are that it is significantly quicker and that it eliminates some of the variability associated with operator or reader input. The tube current used for the CT scan was associated with an effective dose 8 times lower than that associated with a typical diagnostic CT scan. These results suggest that it is possible to segment bone ROIs from low-dose CT images for later transfer to PET images in a single PET/CT procedure without the need for an additional high-resolution CT scan. This technique may aid in understanding the role of bone metabolism in the pathophysiology of osteoporosis and other metabolic bone diseases and may aid in assessing the effects of novel treatments at the femur.

## ACKNOWLEDGMENTS

We thank all the observers who took part in the study from the Diagnostic Imaging Department at the UCD, including Shane Foley, Edel Thomas, Majella McCaffrey, Jonathan McNulty, Joanna Lowe, and Dr. Louise Rainford, and the staff at the PET Imaging Centre at St Thomas' Hospital for their excellent technical support. This work was funded by the Health Research Board in Ireland under grant RP/2007/319. No other potential conflict of interest relevant to this article was reported.

## REFERENCES

- Barbour KE, Zmuda J, Strotmeyer E, et al. Correlates of trabecular and cortical volumetric bone mineral density of the radius and tibia in older men: the Osteoporotic Fractures in Men Study. *J Bone Miner Res.* 2010;25:1017-1028.
- Caulley J, Blackwell T, Zmuda J, et al. Correlates of trabecular and cortical volumetric bone mineral density (vBMD) at the femoral neck and lumbar spine: the osteoporotic fractures in men study (MrOS). *J Bone Miner Res.* 2010;25:1958-1971.
- Piert M, Zittel TT, Becker GA, et al. Assessment of porcine bone metabolism by dynamic [<sup>18</sup>F]fluoride ion PET: correlation with bone histomorphometry. *J Nucl Med.* 2001;42:1091-1100.
- Messa C, Goodman WG, Hoh CK, et al. Bone metabolic activity measured with positron emission tomography and [<sup>18</sup>F]fluoride ion in renal osteodystrophy: correlation with bone histomorphometry. *J Clin Endocrinol Metab.* 1993;77:949-955.
- Cook GJ, Lodge M, Blake G, Marsden P, Fogelman I. Differences in skeletal kinetics between vertebral and humeral bone measured by <sup>18</sup>F-fluoride positron emission tomography in postmenopausal women. *J Bone Miner Res.* 2000;15:763-769.
- Cook GJ, Lodge MA, Marsden PK, Dynes A, Fogelman I. Non-invasive assessment of skeletal kinetics using fluorine-18 fluoride positron emission tomography: evaluation of image and population-derived arterial input functions. *Eur J Nucl Med.* 1999;26:1424-1429.
- Kang Y, Engelke K, Kalender W. A new accurate and precise 3-D segmentation method for skeletal structures in volumetric CT data. *IEEE Trans Med Imaging.* 2003;22:586-598.

8. Pettersson J, Knutsson H, Borga M. Automatic hip bone segmentation using non-rigid registration. In: *ICPR '06 Proceedings of the 18th International Conference on Pattern Recognition*. Volume 3. Washington, DC: IEEE Computer Society; 2006:946–949.
9. Zoroofi RA, Sato Y, Nishii T, et al. Automated segmentation of acetabulum and femoral head from 3-D CT images. *IEEE Trans Inf Technol Biomed*. 2003;7:329–343.
10. Looker AC, Wahner HW, Dunn WL, et al. Proximal femur bone mineral levels of US adults. *Osteoporos Int*. 1995;5:389–409.
11. Damilakis J, Adams J, Guglielmi G, Link T. Radiation exposure in x-ray-based imaging techniques used in osteoporosis. *Eur Radiol*. 2010;20:2707–2714.
12. Ito M, Wakao N, Hida T, et al. Analysis of hip geometry by clinical CT for the assessment of hip fracture risk in elderly Japanese women. *Bone*. 2010;46:453–457.
13. Lang TF, Guglielmi G, van Kuijk C, De Serio A, Cammisa M, Genant HK. Measurement of bone mineral density at the spine and proximal femur by volumetric quantitative computed tomography and dual-energy x-ray absorptiometry in elderly women with and without vertebral fractures. *Bone*. 2002;30:247–250.
14. Bourantas CV, Plissiti ME, Fotiadis DI, et al. In vivo validation of a novel semi-automated method for border detection in intravascular ultrasound images. *Br J Radiol*. 2005;78:122–129.
15. Chalana V, Kim Y. A methodology for evaluation of boundary detection algorithms on medical images. *IEEE Trans Med Imaging*. 1997;16:642–652.
16. Kanis JA, Glüer CC. An update on the diagnosis and assessment of osteoporosis with densitometry. *Osteoporos Int*. 2000;11:192–202.
17. Poole KES, Mayhew PM, Rose CM, et al. Changing structure of the femoral neck across the adult female lifespan. *J Bone Miner Res*. 2010;25:482–491.
18. Colgan N. *Construction and Validation of an Automatic Method for Region of Interest Selection in DMSA Renal Scans*. Sheffield, U.K.: Department of Medical Physics and Clinical Engineering, Sheffield University; 2004.
19. Dice LR. Measures of the amount of ecologic association between species. *Ecology*. 1945;26:297–302.
20. Bartko JJ. Measurement and reliability: statistical thinking considerations. *Schizophr Bull*. 1991;17:483–489.
21. Zijdenbos AP, Dawant BM, Margolin RA, Palmer AC. Morphometric analysis of white matter lesions in MR images: method and validation. *IEEE Trans Med Imaging*. 1994;13:716–724.
22. Xue H, Srinivasan L, Jiang S, et al. Automatic segmentation and reconstruction of the cortex from neonatal MRI. *Neuroimage*. 2007;38:461–477.
23. Akhondi-Asl A, Jafari-Khouzani K, Elisevich K, Soltanian-Zadeh H. Hippocampal volumetry for lateralization of temporal lobe epilepsy: automated versus manual methods. *Neuroimage*. 2010;(suppl 1):S218–S226.
24. Pardoe HR, Pell GS, Abbott DF, Jackson GD. Hippocampal volume assessment in temporal lobe epilepsy: how good is automated segmentation? *Epilepsia*. 2009;50:2586–2592.
25. Sánchez-Benavides G, Gómez-Ansón B, Sainz A, Vives Y, Delfino M, Peña-Casanova J. Manual validation of FreeSurfer's automated hippocampal segmentation in normal aging, mild cognitive impairment, and Alzheimer Disease subjects. *Psychiatry Res*. 2010;181:219–225.
26. Kovalski G, Beyar R, Shofti R, Azhari H. Three-dimensional automatic quantitative analysis of intravascular ultrasound images. *Ultrasound Med Biol*. 2000;26:527–537.
27. Brenner W, Vernon C, Muzi M, et al. Comparison of different quantitative approaches to <sup>18</sup>F-fluoride PET scans. *J Nucl Med*. 2004;45:1493–1500.
28. Brenner W, Vernon C, Conrad E, Eary J. Assessment of the metabolic activity of bone grafts with <sup>18</sup>F-fluoride PET. *Eur J Nucl Med Mol Imaging*. 2004;31:1291–1298.
29. Installé J, Nzeusseu A, Bol A, Depresseux G, Devogelaer J-P, Lonnew M. <sup>18</sup>F-fluoride PET for monitoring therapeutic response in Paget's disease of bone. *J Nucl Med*. 2005;46:1650–1658.
30. Somer EJ, Benatar NA, O'Doherty MJ, Smith MA, Marsden PK. Use of the CT component of PET-CT to improve PET-MR registration: demonstration in soft-tissue sarcoma. *Phys Med Biol*. 2007;52:6991–7006.